Substrate induced composition change during $Ge_2Sb_2Te_5$ atomic layer deposition and study of initial reactions on SiO_2 surface

Jyoti Sinha,[1,2] Laura Nyns,[2] Annelies Delabie [2,1,a]

[1] Department of Chemistry, KU Leuven (University of Leuven), 3001 Leuven, Belgium

[2] IMEC, 3001 Leuven, Belgium

[a)] Electronic mail: annelies.delabie@imec.be

$Ge_2Sb_2Te_5$ (GST) is a well-known phase change material used in non-volatile memory devices, photonics, and non-volatile displays. This study investigates the impact of precursor sequence during the Atomic Layer Deposition of GST from $GeCl_2.C_4H_8O_2$, $SbCl_3$, and $Te[(CH_3)_3Si]_2$ on Si/SiO_2 substrates, focusing on growth per cycle, morphology, and composition along with initial precursor reactions on the substrate. We found that while thick layers approach stoichiometric $Ge_2Sb_2Te_5$, a Ge-rich interfacial layer is initially formed, regardless of the binary ALD sequence used to start the deposition (GeTe versus Sb_2Te_3). Starting the ALD process with the GeTe-Sb_2Te_3 sequence results in a higher Ge content near the GST/SiO_2 interface compared to the Sb_2Te_3-GeTe sequence. To understand these phenomena, we examine the initial precursor reactions on the SiO_2 substrate by total reflection X-ray fluorescence spectrometry. The analysis reveals that $SbCl_3$ exhibits lower reactivity with the SiO_2 substrate than $GeCl_2.C_4H_8O_2$, and not all Ge adspecies react with the $Te[(CH_3)_3Si]_2$ precursors. Additionally, the impact of the initial SiO_2 surface on deposition extends over several ALD cycles, as the SiO_2 surface only gradually gets covered by GST due to island growth. These processes contribute to the formation of a Ge-rich GST layer at the interface, irrespective of the precursor pulse sequence. These insights from the study may contribute to optimizing the

initial deposition stages of GST and other ternary ALD processes to enable better composition control and enhanced device performance.

I. INTRODUCTION

$Ge_2Sb_2Te_5$ (GST) is a phase change material widely studied for its application as a non-volatile memory. The transition of GST from an amorphous to a crystalline state significantly influences its electrical and optical characteristics, which are harnessed for diverse applications. Its application extends beyond non-volatile memory[1–3] to encompass areas such as neuromorphic (brain-inspired) computing[4,5], photonics[6,7], and non-volatile displays[8,9,10]. The need for memory device downscaling has prompted the exploration of atomic layer deposition (ALD) of GST, offering precise control over conformal deposition and composition within complicated device architectures.

GST ALD is a ternary ALD process that consists of the two binary processes of GeTe and Sb_2Te_3[11,12]. The ALD of GST is performed in supercycles by combining the ALD of GeTe and Sb_2Te_3 in a specific cycle ratio to achieve the desired $Ge_2Sb_2Te_5$ phase.[11] Differences in surface chemistry can occur when binary ALD processes are integrated into a ternary ALD process, resulting in differences in growth per cycle (GPC), phase, composition, and morphology of the deposited materials. In addition, ALD-grown GST and GeTe films are amorphous, while ALD-grown Sb_2Te_3 is crystalline. Various Ge, Sb, and Te precursors were utilized for GST deposition.[11–19] $GeCl_2.C_4H_8O_2$, $SbCl_3$, and $Te[(C_2H_5)_3Si]_2$ are utilized by Ritala *et al*.[12] for depositing GST while, Eom *et al*. employed $Ge(OCH_3)_4$, $Sb(OCH_3)_4$, and $Te[(CH_3)_3Si]_2$ as ALD precursors for GST.[18] In GST ALD processes, the reaction sequence typically starts with the binary ALD of GeTe, followed by the ALD of Sb_2Te_3. Nonetheless, it is worth noting that the ALD of GST can be deposited starting with the binary ALD of Sb_2Te_3, followed by the ALD of GeTe (Fig. 1), which may affect the composition, structure, and properties of the films. Indeed, if the two binary ALDs have different surface reactivity towards

the starting substrate, this might affect the composition of the ternary material near the substrate. In previous work, we observed a Ge-rich interfacial layer near the interface for GST ALD on SiO_2 and TiN substrates, while thick layers approached stoichiometric $Ge_2Sb_2Te_5$.[19] In this case, the ternary ALD of GST started with the binary GeTe ALD sequence, followed by the Sb_2Te_3 ALD sequence. Consequently, it would be interesting to explore the impact of initiating the ALD of GST with Sb_2Te_3 on GST composition, as this may help control the concentration of Ge near the interface. Moreover, the difference in reactivity of binary ALDs towards the substrate can affect the structure and morphology of ternary material.

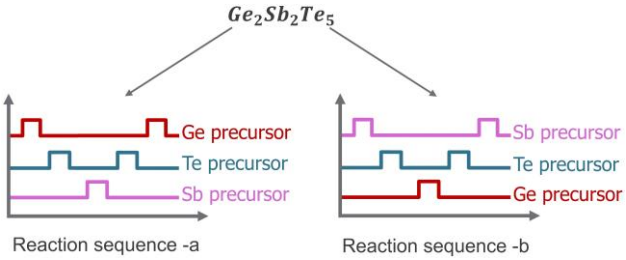

FIG. 1. Schematic showing two different ALD sequences for GST.

This study investigates the initial stages during the Atomic Layer Deposition of GST films from $GeCl_2.C_4H_8O_2$, $SbCl_3$, and $Te[(CH_3)_3Si]_2$ on Si/SiO_2 substrates and the impact on growth per cycle, morphology, and composition. We investigate the impact of the ALD sequences (GeTe-Sb_2Te_3 versus Sb_2Te_3-GeTe) on the ternary ALD GST process. In addition, we investigate the initial ALD reactions and the layer closure of GST ALD on the Si/SiO_2 substrate. Based on the results, we discuss mechanisms that are consistent with the formation of a Ge-rich interfacial layer.

II. EXPERIMENTAL

A. Materials and Processing

300 mm Si wafers were utilized for the deposition process. Before GST deposition, SiO_2 was deposited at 75 °C in the ASM Eagle 12 chamber using plasma-enhanced atomic layer

deposition (PEALD) to achieve a 20 nm film. Subsequently, GST deposition was conducted in an ASM Pulsar 3000 crossflow reactor connected to a Polygon platform at 70 °C, according to conditions as described previously.[19,20] $GeCl_2.C_4H_8O_2$, $SbCl_3$, and $Te[(CH_3)_3Si]_2$ were used as precursors. $GeCl_2.C_4H_8O_2$ was heated to 80 °C to maintain adequate vapor pressure, while $SbCl_3$ and $Te[(CH_3)_3Si]_2$ were maintained at room temperature. The cycle ratio of GeTe and Sb_2Te_3 was always maintained as 2:3.[19] The GST deposition was performed in two ways. In the first way, deposition is initiated with GeTe, having two ALD cycles of GeTe, followed by three cycles of Sb_2Te_3 in one supercycle of GST. These ALD depositions were done for different cycles where GeTe is deposited first. In other way, deposition is initiated with Sb_2Te_3, having three ALD cycles of Sb_2Te_3, followed by two cycles of GeTe in one supercycle of GST. However, GST deposition initiated with Sb_2Te_3 was performed only for 8 and 36 cycles, with the latter corresponding to complete substrate coverage during film deposition.

B. Characterization

The mass was measured before and after GST deposition in Metryx Metior 3000 to estimate growth per cycle (GPC). X-ray reflectivity (XRR) was done to determine the density in a JVX7300M tool from Jordan Valley, followed by XRR fitting based on a GeO_2/GST/SiO_2/Si stack. The morphology of GST was investigated using a scanning electron microscope (SEM) in a FEI Helios 460 microscope, operating with a 3 kV/0.1 nA incoming beam and a secondary electron detector. The composition of GST was assessed with the help of X-ray fluorescence spectrometry (XRF) in a PANalytical 2830 ZT. Total reflection X-ray fluorescence spectrometry (T-XRF) was utilized to measure concentrations of adsorbed precursors on SiO_2, which was performed in a Rigaku TXRF300 system. In the case of T-XRF, the incident angle is kept low so that it only grazes the surface, and the surface sensitivity can be increased to measure the concentration of elements adsorbed on the surface. Time of flight secondary ion mass spectrometry (TOF-SIMS) was employed to investigate the composition

of GST along the thickness. This was conducted in an ION-TOF GmbH using Bi^{1+} as the analysis beam and Cs^{+} as the sputtering beam.

III. RESULTS AND DISCUSSION

A. ALD of GST

First, we investigate the impact of the starting precursor on the GST thickness, morphology, and composition by comparing GST films deposited with the GeTe-Sb_2Te_3 ALD sequence, starting with the $GeCl_2.C_4H_8O_2$ reaction (GST-a), with GST films deposited with Sb_2Te_3-GeTe ALD sequence, starting with the $SbCl_3$ reaction (GST-b). Fig. 2(a) compares the mass gain of GST as a function of the number of ALD cycles. Initially, at 8 cycles, GST-a and GST-b show a similar mass gain. However, at 36 cycles, GST-a has a slightly higher mass gain than GST-b, while both GST-a and GST-b have a similar density of 5.6 g/cm^3. Similar to our prior research, wherein we observed amorphous ALD GST (~20 nm) on SiO_2 using transmission electron microscopy,[19] the calculated densities of GST on SiO_2 are lower than the crystalline GST, ascertaining the amorphous nature of GST. Consequently, the difference in mass gain implies a difference in thickness. The thickness of GST-a corresponds to 9 nm after 36 cycles, while the thickness of GST-b is only 8 nm. The growth per cycle (GPC) of GST-a is 128 μg/cycle, which is higher than the GPC of GST-b of 101 μg/cycle. This difference in thickness indicates that the order of the sequences of binary ALD cycles affects the initial surface reaction chemistry, resulting in the difference in mass gain and thickness.

In contrast, we do not observe a significant impact of the starting precursor on morphology after 8 and 36 ALD cycles, as indicated by the SEM images in Fig. 2(b).

Furthermore, the composition of GST was investigated using XRF (Fig. 3(a)) and TOF-SIMS depth profiles (Fig. 3(b)). According to XRF, the GST-a and GST-b thin films (8 cycles) are Ge-rich. These findings highlight that GST initially exhibits a Ge-rich composition,

regardless of the starting precursor in the ALD reaction cycle. Still, the starting precursor affects the composition as we observe a 15 percent higher Ge concentration in GST-a compared to GST-b at 8 cycles. Both GST-a and GST-b films reach the desired 2:2:5 GST composition at 36 cycles, with the film thickness of 9 nm and 8 nm, respectively. Fig. 3(b) displays the TOF-SIMS Ge/Sb intensity ratio for GST-a and GST-b. The ratio of Ge/Sb in the GST bulk is similar for both GST-a and GST-b. However, close to the GST/SiO_2 interface, the Ge/Sb ratio is higher for GST-a as compared to GST-b, indicating that starting the deposition with a $GeCl_2.C_4H_8O_2$ reaction results in a higher Ge content in the Ge-rich layer near the GST/SiO_2 interface. These results are in accordance with the XRF findings.

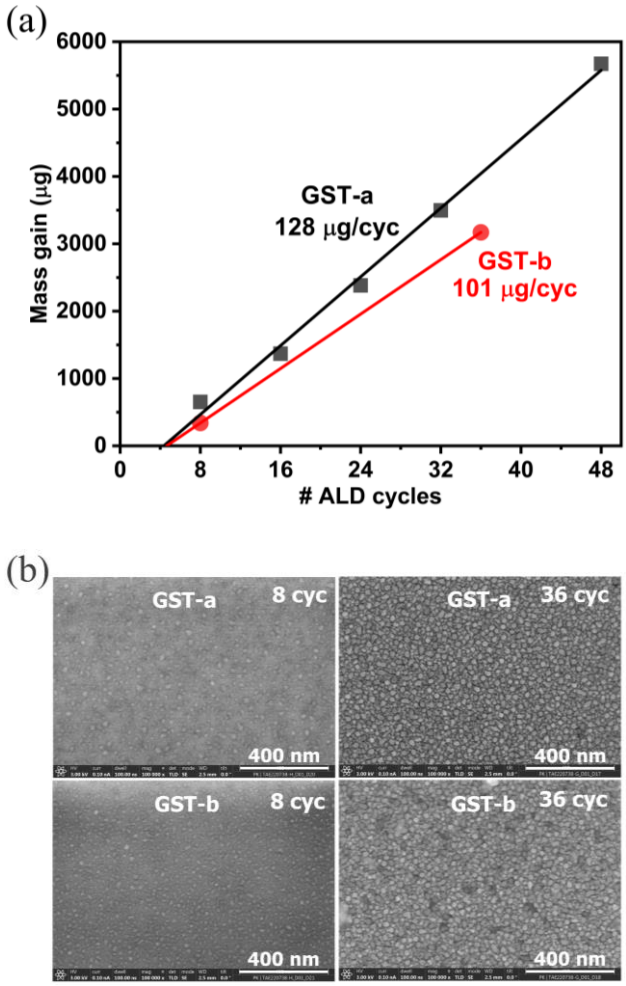

FIG. 2. (a) Mass gain for GST-a and GST-b with ALD cycles. (b) SEM micrographs showing the morphology of GST-a and GST-b deposited at 8 and 36 cycles.

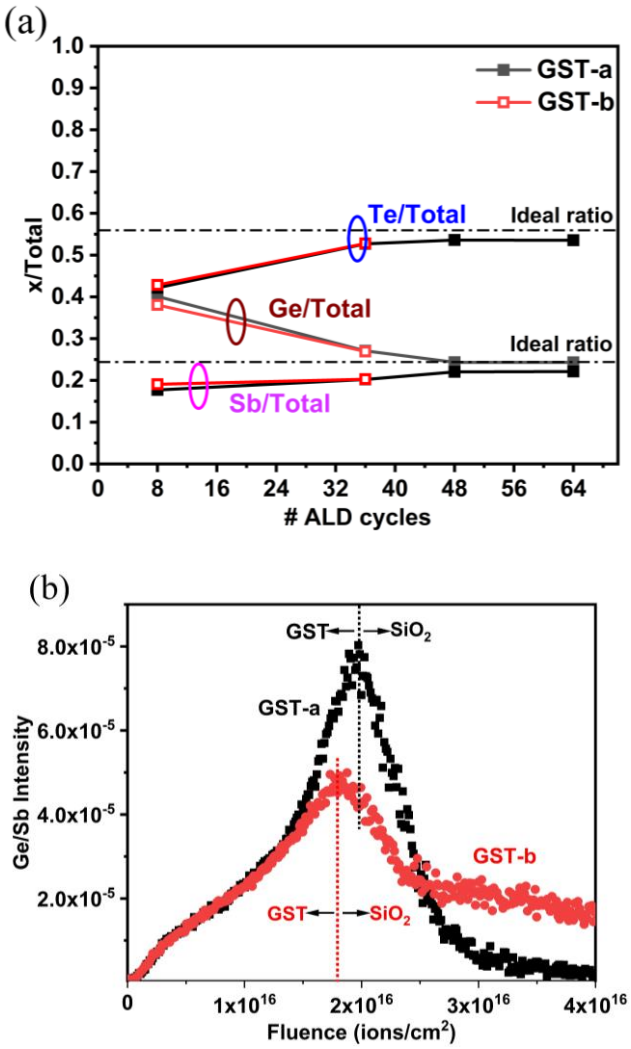

FIG. 3. (a) Ratio of Ge, Sb, and Te to total concentration on GST-a and GST-b determined through XRF. (b) The ratio of Ge and Sb on GST-a and GST-b along thickness deposited at 36 cycles. The black dotted line shows the GST-a and SiO_2 interface, and the red dotted line shows GST-b and SiO_2 interface. (It is to note that the difference in ratio from TOF-SIMS will not present the actual difference in composition as it is dependent on elements and matrix effect.)

B. Investigation of initial precursor reactions on the Si/SiO_2 substrate

The difference in thickness and composition relates to the initial surface chemistry of precursors and their interaction with the SiO_2 surface. Thus, further investigation of the initial surface reactions is crucial to understand the reactions on the SiO_2 surface and their effect on

the thickness and composition of the GST films. To better understand the formation of the Ge-rich interfacial layer and the impact of the order of the reactions, we investigate the initial reactions of the ALD precursors on the SiO_2 substrate.

1. $GeCl_2.C_4H_8O_2$ and $SbCl_3$ reactions on the initial SiO_2 substrate

The $GeCl_2.C_4H_8O_2$ and $SbCl_3$ precursors are first pulsed individually on the SiO_2 substrate. The pulse durations are varied to verify the self-limiting nature of the reactions on the initial SiO_2 substrate, as the dose required to saturate the initial substrate may be different than during bulk growth. The Ge and Sb content were verified by T-XRF. A single saturated reaction of $GeCl_2.C_4H_8O_2$ on the SiO_2 substrate leads to 1.26 Ge at/nm^2 (Table 1, Fig. 4(a)). The Ge-content is ~ 4 times higher than the Sb-content from a single saturated $SbCl_3$ reaction on a SiO_2 substrate (0.29 at/nm^2) for the same pulse duration of 80 seconds (Fig. 4(a)). The difference in concentration highlights the different reactivity of $GeCl_2.C_4H_8O_2$ and $SbCl_3$ towards the SiO_2 surface: $GeCl_2.C_4H_8O_2$ is more reactive than $SbCl_3$ on the initial SiO_2 surface, consistent with the enrichment of the Ge-content near the interface with the SiO_2 substrate.

Also, a long purge time of 120 seconds was considered after the $GeCl_2.C_4H_8O_2$ and $SbCl_3$ reactions to evaluate the type of absorption on SiO_2. Fig. 4(b) shows no significant effect of the longer purge times on the concentrations of Ge and Sb, suggesting that both $GeCl_2.C_4H_8O_2$ and $SbCl_3$ chemisorb on the SiO_2 surface.

TABLE 1. The concentration of different elements observed during precursor pulse.

Precursor pulse	**Ge (at/nm^2)**	**Te (at/nm^2)**	**Sb (at/nm^2)**
$GeCl_2.C_4H_8O_2$	1.26		
$GeCl_2.C_4H_8O_2$-$Te[(CH_3)_3Si]_2$	1.4	0.37	
$GeCl_2.C_4H_8O_2$-$Te[(CH_3)_3Si]_2$-$SbCl_3$	0.86	0.09	0.06
$SbCl_3$			0.13
$SbCl_3$-$Te[(CH_3)_3Si]_2$		0.1	0.14
$SbCl_3$-$Te[(CH_3)_3Si]_2$-$GeCl_2.C_4H_8O_2$	1	0.41	0.12

2. $Te[(CH_3)_3Si]_2$ reaction on $GeCl_2.C_4H_8O_2$ and $SbCl_3$ treated SiO_2

To better understand the impact of the initial substrate, we also consider different sequential precursor reactions. When we pulse $GeCl_2.C_4H_8O_2$ and $Te[(CH_3)_3Si]_2$ sequentially on the SiO_2 substrate, we find that the concentration of Te (0.37 at/nm^2) is almost 4 times lower than the concentration of Ge (1.4 at/nm^2) (Fig. 4(c)). Similarly, in the $GeCl_2.C_4H_8O_2$-$Te[(CH_3)_3Si]_2$-$SbCl_3$ sequence, the concentration of Te (0.09 at/nm^2) is much lower than that of Ge (0.86 at/nm^2) (Fig. 4(d)). Thus, the stoichiometry of the $Te[(CH_3)_3Si]_2$ reaction is surface dependent: it is different on the $GeCl_2.C_4H_8O_2$ treated SiO_2 surface than on a GeTe surface during ALD. The Ge/Te ratio for the $Te[(CH_3)_3Si]_2$ reaction proposed for GeTe ALD bulk growth, based on in-situ investigations, is 1.4 (equation 1) [21]:

$$-Te_{0.7}GeCl_{1.3}(s) + Te((C_2H_5)_3Si)_2(g) \rightarrow -TeGe[Te(Si(C_2H_5)_3)]_{0.7}(s) + 1.3(C_2H_5)_3SiCl(g) \quad (1)$$

The deviation from 1:1 stoichiometry and the excess of Ge for the reactions on the initial SiO_2 substrate is consistent with the formation of the Ge-rich interfacial layer and indicates that not all Ge adspecies react with $Te[(CH_3)_3Si]_2$ during the first reaction cycle. The reaction of the $Te[(CH_3)_3Si]_2$ precursor could be limited by the availability of Cl on the surface after the $GeCl_2.C_4H_8O_2$ reaction. We note that quantifying the Cl-content could reveal the reaction stoichiometry of the metal chloride surface reactions with the $Te[(CH_3)_3Si]_2$. Unfortunately, quantifying the Cl content is not possible by T-XRF as the measurements are performed ex-situ, and Cl surface species hydrolyze quickly when exposed to the air environment. Therefore, it is difficult to verify the reaction stoichiometry by T-XRF further.

Similarly, the concentrations of Sb and Te were investigated when the $SbCl_3$ and $Te[(CH_3)_3Si]_2$ precursors were pulsed sequentially (Table 1). However, Sb/Te ratio in the $SbCl_3$-$Te[(CH_3)_3Si]_2$ and $SbCl_3$-$Te[(CH_3)_3Si]_2$-$GeCl_2.C_4H_8O_2$ sequences are slightly different, complicating further discussion.

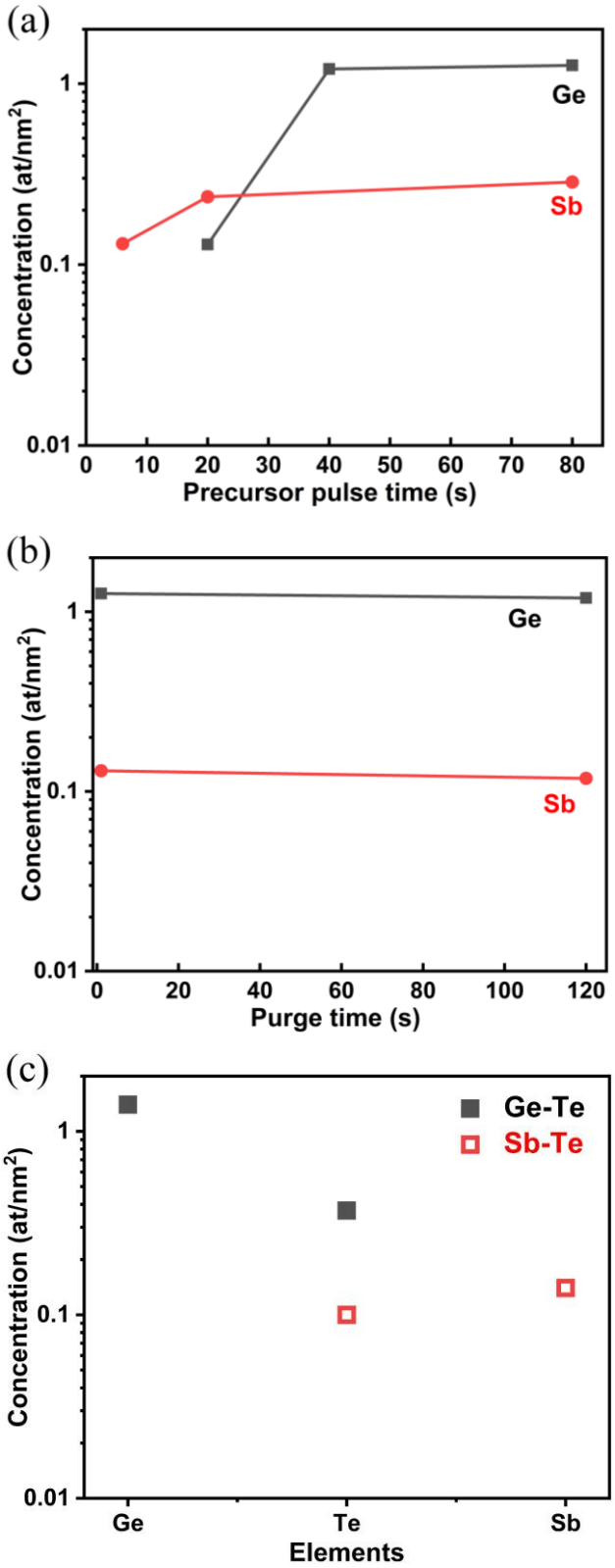
(a)
Concentration (at/nm²)
1
0.1
0.01
0
10
20
30
40
50
60
70
80
Precursor pulse time (s)
Ge
Sb
(b)
Concentration (at/nm²)
1
0.1
0.01
0
20
40
60
80
100
120
Purge time (s)
Ge
Sb
(c)
Concentration (at/nm²)
1
0.1
0.01
Ge
Te
Sb
Elements
Ge-Te
Sb-Te

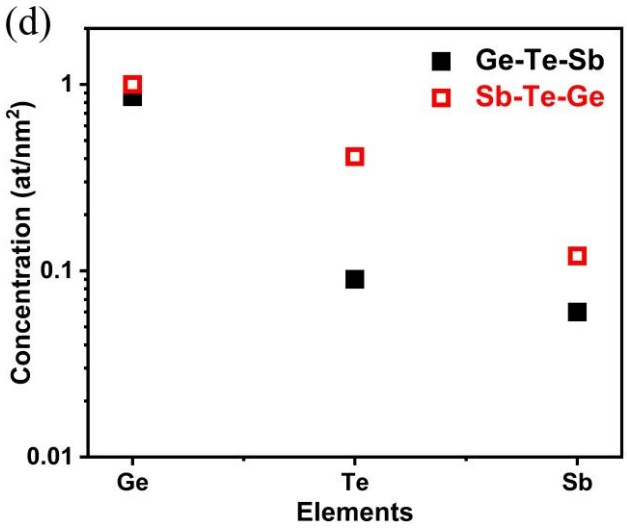

FIG. 4. Graph showing the concentration of Ge and Sb with different (a) pulse times and (b) purge times. The concentration of Ge, Te, and Sb when reactions have precursor sequence of (c) $GeCl_2.C_4H_8O_2$-$Te[(CH_3)_3Si]_2$ (Ge-Te) and $SbCl_3$-$Te[(CH_3)_3Si]_2$ (Sb-Te) and, (d) $GeCl_2.C_4H_8O_2$-$Te[(CH_3)_3Si]_2$-$SbCl_3$ (Ge-Te-Sb) and $SbCl_3$-$Te[(CH_3)_3Si]_2$- $GeCl_2.C_4H_8O_2$ (Sb-Te-Ge) on SiO_2.

3. *$GeCl_2.C_4H_8O_2$ and $SbCl_3$ reactions on $SbCl_3$-$Te[(CH_3)_3Si]_2$ and $GeCl_2.C_4H_8O_2$-$Te[(CH_3)_3Si]_2$ treated SiO_2*

The Ge content (~1 at/nm^2) is similar for all investigated reaction sequences (Table 1). On the other hand, the $SbCl_3$ reaction is affected by the surface composition. The concentration of Sb (0.06 at/nm^2) after a $GeCl_2.C_4H_8O_2$-$Te[(CH_3)_3Si]_2$-$SbCl_3$ sequence is even lower than the Sb concentration after the $SbCl_3$ reaction on the initial SiO_2 substrate (0.13 at/nm^2). This indicates that $SbCl_3$ adsorption depends on the surface composition and that $SbCl_3$ adsorption occurs more slowly in the presence of adspecies resulting from the $GeCl_2.C_4H_8O_2$-$Te[(CH_3)_3Si]_2$ sequence on the SiO_2 substrate.

We conclude that the high Ge/Te ratio after the $Te[(CH_3)_3Si]_2$ reaction and the lower overall reactivity of $SbCl_3$ versus $GeCl_2.C_4H_8O_2$ in the early stages of the ALD process are consistent with the formation of a Ge-rich interfacial layer during GST ALD.

C. *Theoretical modelling for $GeCl_2.C_4H_8O_2$-$Te[(CH_3)_3Si]_2$-$SbCl_3$ and $SbCl_3$-$Te[(CH_3)_3Si]_2$- $GeCl_2.C_4H_8O_2$*

A theoretical model will be explored using T-XRF results to understand the initial reactions during GST ALD. Our model is based on the following assumptions. The first assumption is that only ligand exchange reactions occur during ALD, as illustrated in Fig. 5(a) for the $SbCl_3$ reaction. Second, only the hydroxyl (OH) groups on the SiO_2 substrate are assumed to be the initially present reactive sites for ligand exchange reactions. In addition, we ignore surface diffusion and aggregation of adspecies on the SiO_2 surface. These assumptions align with the reactivity of other metal chloride precursors with hydroxylated SiO_2 substrates during ALD.[22,23]

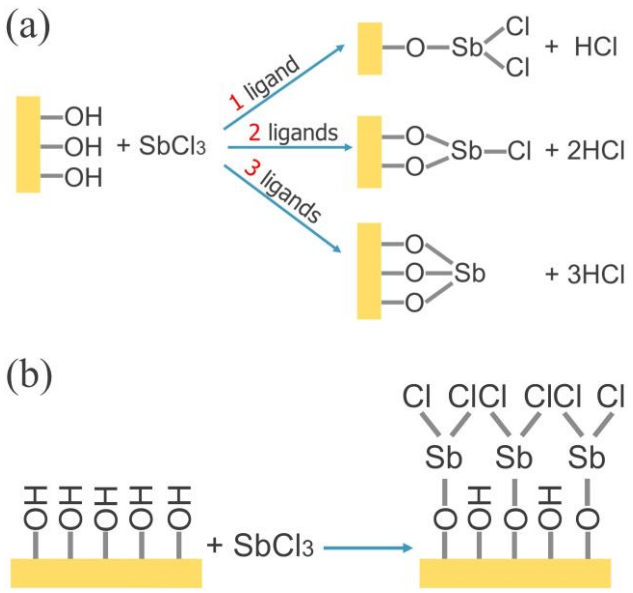

FIG. 5. Schematic showing (a) ligand exchange reactions and (b) effect of steric hindrance.

Different types of ligand exchange reactions of $GeCl_2.C_4H_8O_2$ can occur on SiO_2 surface: $GeCl_2.C_4H_8O_2$ can react with one OH group, and/or $GeCl_2.C_4H_8O_2$ can react with two OH groups. We also assume that the adduct of $GeCl_2$, $C_4H_8O_2$, is detached before $GeCl_2$ adsorbs on the SiO_2 surface as it is weakly bonded.[21] Therefore, the hydroxyl density required for ligand exchange reaction can be estimated from the Ge content as measured by TXRF. If a ligand

exchange reaction occurs with one OH group per $GeCl_2.C_4H_8O_2$ molecule, the concentration of reacted OH groups will equal the Ge content after the reaction, i.e., 1.26 – 1.40 at/nm^2. If a ligand exchange reaction occurs with two OH groups per $GeCl_2.C_4H_8O_2$ molecule, the concentration of active sites will be 2 times higher, i.e. 2.52 – 2.80 at/nm^2. In previous studies, it is found that the concentration of OH groups on SiO_2 deposited by PEALD is 2.5 at/nm^2.[24] Therefore, the number of OH groups on SiO_2 will be sufficient not to limit ligand exchange reactions, as it would only become a limiting factor when all $GeCl_2$ molecules react with two OH groups.

Similarly, in the case of $SbCl_3$, the hydroxyl densities needed to enable complete ligand exchange reactions of one, two, or three Cl-ligands per $SbCl_3$ molecule are 0.29 at/nm^2, 0.58 at/nm^2, or 0.87 at/nm^2, respectively. These hydroxyl densities are calculated from the Sb content as measured by T-XRF and the reaction stoichiometry. Since these OH densities are much lower compared to those required for reaction with $GeCl_2.C_4H_8O_2$, hinting towards more unreacted sites on the surface when starting the deposition with an $SbCl_3$ reaction.

We also examine the effect of steric hindrance during the ligand exchange reactions on the SiO_2 substrate. When $GeCl_2$ or $SbCl_3$ react through ligand exchange reactions, steric hindrance from the Cl ligands can limit the reaction (Fig. 5(b)). To estimate the Cl content at the limit of steric hindrance, a hexagonal packing and ionic radius of Cl have been assumed, resulting in the maximum concentration of Cl corresponding to 8.8 at/nm^2.[23,25] Based on this, we have calculated the minimum concentration of Ge and Sb required for steric hindrance to limit the reaction as shown in Table 2. It is evident that the actual concentrations of both Ge (1.26 at/nm^2) and Sb (0.29 at/nm^2) are insufficient to approach the limit of steric hindrance during ligand exchange reaction. Therefore, while investigating reaction pathways, steric hindrance is not considered to be a limiting factor.

TABLE 2. The minimum concentration of Ge and Sb required to apply steric hindrance.

No of ligand exchange	0 (at/nm^2)	1 (at/nm^2)	2 (at/nm^2)	Actual con. (at/nm^2)
Con. of Ge	4.4	8.8		1.26
Con. of Sb	2.9	4.4	8.8	0.29

To determine the reaction pathway for $GeCl_2.C_4H_8O_2$ on SiO_2, we evaluate the Te content during the sequential reaction with $Te[(CH_3)_3Si]_2$. Since Te was detected in T-XRF, this indicates that $Te[(CH_3)_3Si]_2$ has reacted with an -GeCl surface site. This eliminates the possibility of $GeCl_2.C_4H_8O_2$ reacting only with two OH groups, as no Cl would be left to react with the incoming $Te[(CH_3)_3Si]_2$ precursor (Fig. 6(a)). Hence, we propose that $GeCl_2$ reacts with hydroxyl groups either by a one ligand exchange reaction or the combination of one and two ligand exchange reactions, as shown in Fig. 6(a). This can also explain why the concentration of Ge is ~4 times higher than the concentration of Te, as the $Te[(CH_3)_3Si]_2$ reaction is limited by the availability of Cl on the surface due to the high reactivity of $Te[(CH_3)_3Si]_2$ with surface -Cl.[11,26] From the Te-content (0.37 Te/nm^2) and the Ge-content (1.4 Ge/nm^2), we conclude that 74 percent of Ge adspecies have not reacted and the possible reaction mechanism for $GeCl_2.C_4H_8O_2$- $Te[(CH_3)_3Si]_2$ are illustrated in Fig. 6(b). This reaction model can be consistent with the Ge-rich GST layer in the initial ALD cycles.

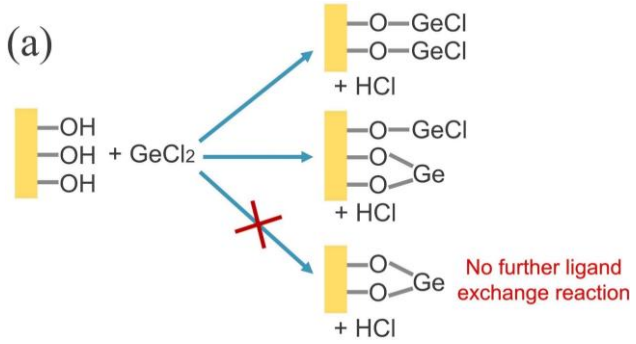

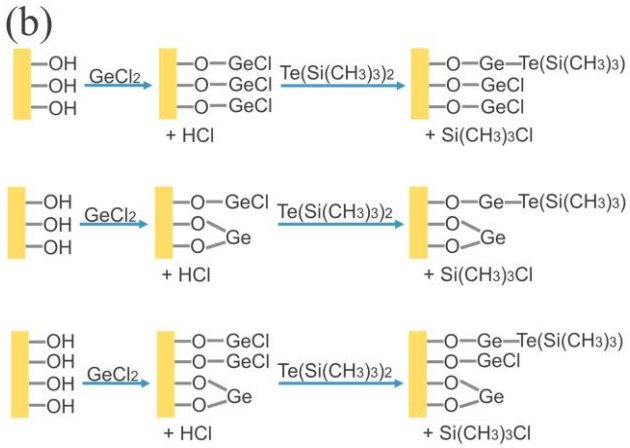

FIG. 6. Possible reaction mechanism (a) for $GeCl_2$ chemisorbed on SiO_2 based on the experimental observation of $GeCl_2.C_4H_8O_2$-$Te[(CH_3)_3Si]_2$. (b) Schematic showing possible reaction pathway for the $GeCl_2.C_4H_8O_2$-$Te[(CH_3)_3Si]_2$ ($GeCl_2.C_4H_8O_2$ is written as $GeCl_2$ in reaction mechanism).

Correspondingly, the reaction mechanism for the $SbCl_3$-$Te[(CH_3)_3Si]_2$ sequence is deduced from the experimental findings of the reaction of $SbCl_3$ and $SbCl_3$-$Te[(CH_3)_3Si]_2$ on SiO_2. The presence of Te in T-XRF observation eliminates the possibility of only three ligand exchange reactions of $SbCl_3$ with SiO_2 as it leaves no Cl for further reaction with $Te[(CH_3)_3Si]_2$ (Fig. 5(a)). If it is assumed that only one or two ligand exchange reactions are taking place with $SbCl_3$ on SiO_2, followed by only one ligand exchange reaction with $Te[(CH_3)_3Si]_2$, then also the Te content would be 0.28 at/nm^2 or 1.4 at/nm^2 respectively. In either case, Te content is higher than experimental findings, indicating that some chemisorbed Sb will be unreacted (Fig. 7). The unreacted Sb can be present with one or two Cl ligands or combinations of both. In any case, an Sb-rich layer will be present near the interface in the initial ALD cycles. This observation differs from the TOF-SIMS results, as we observe a Ge-rich interface regardless of whether the ALD reaction starts with the GeTe-Sb_2Te_3 or Sb_2Te_3-GeTe sequence.

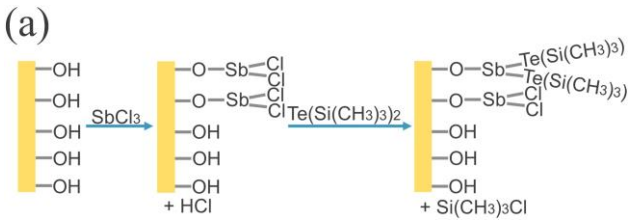

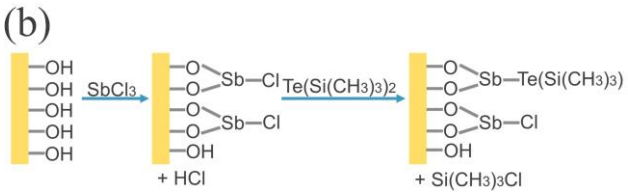

FIG. 7. Schematic showing possible reaction pathway for the $SbCl_3$-Te[$(CH_3)_3Si]_2$ sequence where only (a) one and (b) two ligand exchange reactions take place.

Furthermore, based on the experimental T-XRF and the stated reaction pathway for $GeCl_2.C_4H_8O_2$-Te[$(CH_3)_3Si]_2$ and $SbCl_3$-Te[$(CH_3)_3Si]_2$ above, the deduction of the possible reaction mechanism for $GeCl_2.C_4H_8O_2$-Te[$(CH_3)_3Si]_2$-$SbCl_3$ and $SbCl_3$-Te[$(CH_3)_3Si]_2$-$GeCl_2.C_4H_8O_2$ is quite complicated. In the case of $GeCl_2.C_4H_8O_2$-Te[$(CH_3)_3Si]_2$-$SbCl_3$, the concentration of Te is ~10 times higher than that of Ge. Considering only one ligand exchange reaction between $GeCl_2$ and Te[$(CH_3)_3Si]_2$, around 90 percent of Ge is unreacted with Te[$(CH_3)_3Si]_2$, irrespective of any reaction pathway. Fig.8(a) and 8(b) depict two possible reaction pathways out of many possibilities where the unreacted Ge can be present as -OGeCl or the combination of -OGeCl and -OGeO-. Either of them could be responsible for the high concentration of Ge at the interface of GST-a with SiO_2, resulting in Ge-rich GST.

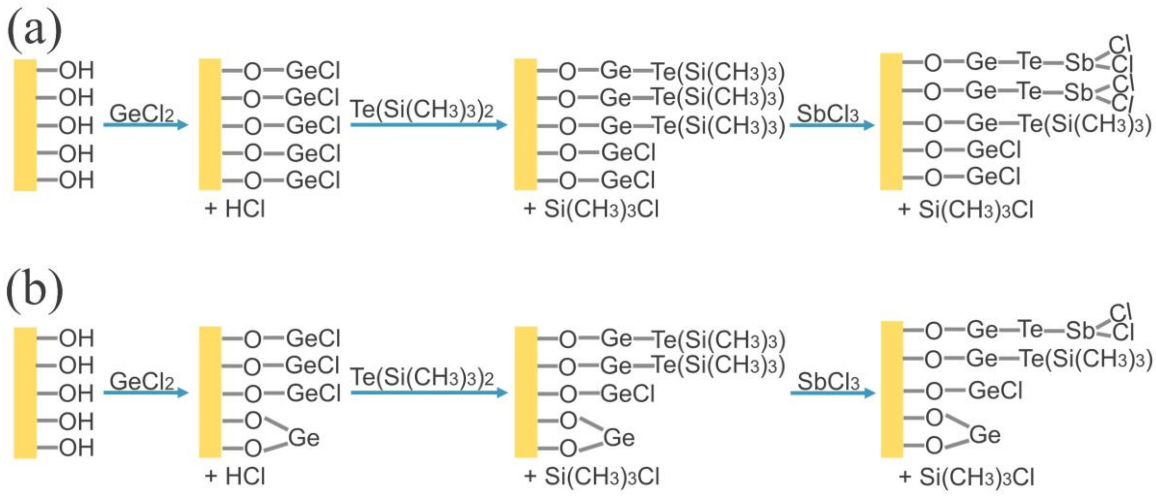

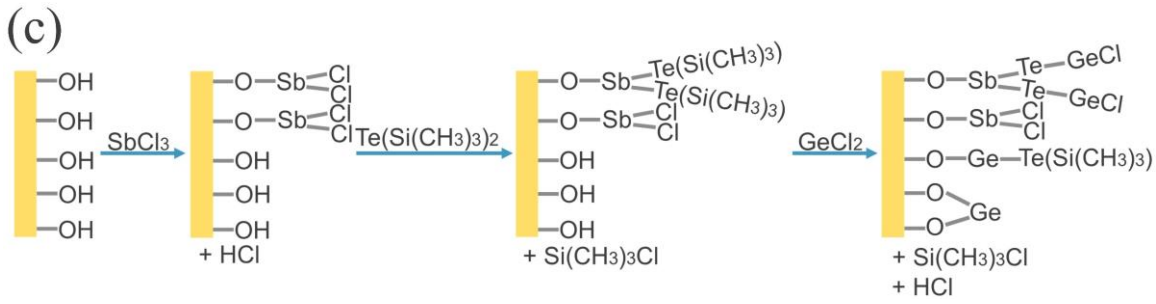

FIG. 8. Schematic showing possible reaction pathway for the reaction of $GeCl_2.C_4H_8O_2$-$Te[(CH_3)_3Si]_2$-$SbCl_3$ where $GeCl_2$ went for (a) only one and (b) combination of one and two ligand exchange reactions with SiO_2. (c) Reaction pathway of $SbCl_3$-$Te[(CH_3)_3Si]_2$-$GeCl_2.C_4H_8O_2$ where $SbCl_3$ went for one ligand exchange reaction and showing chemisorbed Ge on available sites of SiO_2 ($GeCl_2.C_4H_8O_2$ is written as $GeCl_2$ in reaction mechanism).

Similar to the reaction sequence of $GeCl_2.C_4H_8O_2$-$Te[(CH_3)_3Si]_2$, it is not straightforward to deduce the reaction pathway for $SbCl_3$-$Te[(CH_3)_3Si]_2$-$GeCl_2.C_4H_8O_2$ based on experimental findings. For $SbCl_3$-$Te[(CH_3)_3Si]_2$-$GeCl_2.C_4H_8O_2$, it is found that the concentration of Ge (1 at/nm^2) is ~8 times higher than that of Sb (0.12 at/nm^2), which would be not possible with only one ligand exchange reaction of $SbCl_3$ on SiO_2. The one ligand exchange reaction of $SbCl_3$ with SiO_2 results in maximum Cl for the incoming precursor, leading to the maximum Ge/Sb ratio of 2, which is lower than that of the experimental findings. Therefore, we propose that during the pulse of $GeCl_2.C_4H_8O_2$ in $SbCl_3$-$Te[(CH_3)_3Si]_2$-$GeCl_2.C_4H_8O_2$, some $GeCl_2$ chemisorbed on available OH sites (Fig. 8(c)). As asserted above, the number of active sites (~2.5 at/nm^2) is sufficient, and some active sites remain available even with the chemisorbed Sb (0.12 at/nm^2). These available surface sites provide the opportunity for incoming Ge precursor molecules to chemisorbed on SiO_2, which could account for the higher Ge concentration for $SbCl_3$-$Te[(CH_3)_3Si]_2$-$GeCl_2.C_4H_8O_2$ reaction sequence. Similar to the Ge/Sb ratio, considering only one ligand exchange for $SbCl_3$ with SiO_2 for maximum Cl, the Te/Sb ratio would be 2, which is lower than the observed ratio of 3.4. Therefore, we hypothesize that some $Te[(CH_3)_3Si]_2$ remains in the chamber during the pulse of $GeCl_2.C_4H_8O_2$, which can react with chemisorbed Ge on SiO_2 (Fig. 8(c)). However, the

concentration of Ge is ~3 times higher than the concentration of Te, which leaves 59 percent of the total Ge concentration unreacted with $Te[(CH_3)_3Si]_2$. Considering only one ligand exchange reaction between $GeCl_2$ and $Te[(CH_3)_3Si]_2$, 59 percent of unreacted Ge will be present irrespective of the reaction pathway. However, it is essential to mention the limitation of the proposed reaction pathway. In both reaction sequences of $GeCl_2.C_4H_8O_2$-$Te[(CH_3)_3Si]_2$-$SbCl_3$ and $SbCl_3$-$Te[(CH_3)_3Si]_2$-$GeCl_2.C_4H_8O_2$, illustrated in Fig. 8, the unreacted Ge can be present as -OGeCl or -OGeO- or a combination of both because the reactivity of Te precursors with chemisorbed Ge cannot be accurately determined due to the absence of Cl during T-XRF measurement. Therefore, determining the concentration of each surface species is difficult with the existing experimental setup.

In conclusion, the presence of Ge surface species unreactive towards $Te[(CH_3)_3Si]_2$ can explain the formation of a Ge-rich GST layer in the initial ALD cycles on SiO_2. Moreover, the difference in reactivity of $GeCl_2.C_4H_8O_2$ and $SbCl_3$ precursor towards SiO_2 facilitates the prospect for $GeCl_2.C_4H_8O_2$ to react with available active sites, resulting in Ge-rich GST, even when ALD starts with $SbCl_3$. A Ge-rich interfacial layer was previously also observed for a different GST ALD process at 70 °C based on $HGeCl_3$ and $Sb(OC_2H5)_3$.[15] In that case, it was proposed that replacement of Sb with Ge leads to the Ge-rich interfacial layer.[15] Our results in Table 1 do not support the replacement of Sb with Ge, indicating that the reaction mechanisms are precursor dependent. Further investigations, for example, using in-situ measurements, could provide further details on the reaction mechanisms during the early stages of GST ALD. It would be appropriate to consider different precursors, substrates, temperatures, and a greater number of ALD cycles, as well as additional reactions next to the ligand exchange reaction, to get more insight.

D. GST ALD growth mode and layer closure

Finally, we investigate how fast the SiO_2 surface gets covered by GST, as this will determine during how many ALD cycles the SiO_2 surface is exposed to the ALD precursors. We do not observe a significant impact of the starting precursor on the morphology. At 8 cycles, the GST film does not seem to cover the substrate fully, irrespective of the binary ALD sequence used to start the deposition (GeTe versus Sb_2Te_3). Hence, we performed a GST layer closure analysis using static TOF-SIMS surface analysis to understand the surface morphology and its evolution during ALD.[27–29] Fig. 9(a) shows that the Si intensity, which relates to the concentration of Si near the top surface of the sample, decreases as the GST film thickness increases, consistent with GST deposition. The exponential decay of the Si signal intensity is fitted according to the following equation:

$$I/Io = \exp(-t/\lambda)^{27,29} \quad (2)$$

I is the TOF-SIMS substrate signal intensity, Io is the intensity of the substrate signal on a sample with no deposition, t is the thickness, and λ is a parameter that relates to how fast the surface gets covered.[27,29] The λ is fitted to 1.26 nm. The high λ value indicates a slow decay and implies that island growth of GST takes place (Fig. 2(b)). This is in line with the growth inhibition during the first ALD cycles, as observed from mass gain (Fig. 2(a)). The Si signal intensity saturates when the film fully covers the SiO_2 surface. This saturation and, hence, surface closure of GST is seen at an average film thickness of 6 nm (~24 cycles). Note that GST samples have been oxidized due to air exposure, so the actual thickness for surface closure may be affected slightly by surface oxidation (1-2 nm).

As the SiO_2 surface is covered only completely after 24 cycles, the precursors may reach and react with the remaining SiO_2 surface area during the initial 24 cycles. This would imply that the surface reactions that lead to the Ge-enrichment can continue during the first 24 cycles.

Indeed, it is interesting to note in Fig. 9(a) that Ge-rich GST reaches the desired 2:2:5 composition near the point where the surface gets closed, i.e., 6 nm.

The overall qualitative mechanism is schematically represented in Fig. 9(b). As long as the initial SiO_2 surface remains uncovered, i.e., during the first 24 ALD cycles, the precursor reactions on the SiO_2 surface area enable the formation of a Ge-rich interlayer. The higher reactivity of $GeCl_2.C_4H_8O_2$ versus $SbCl_3$ towards the SiO_2 surface and the formation of unreactive Ge surface species during the GeTe process sequence continues to play a role as long as parts of the SiO_2 surface remain uncovered. This leads to the formation of a Ge-rich GST/SiO_2 interface.

This mechanism can also explain why the starting sequence in the ALD process plays a small role: the Ge enrichment continues on the exposed SiO_2 surface area irrespective of the starting sequence in the ALD process, resulting in only 15 percent difference in initial Ge-content for the GeTe-Sb_2Te_3 and Sb_2Te_3-GeTe starting sequences.

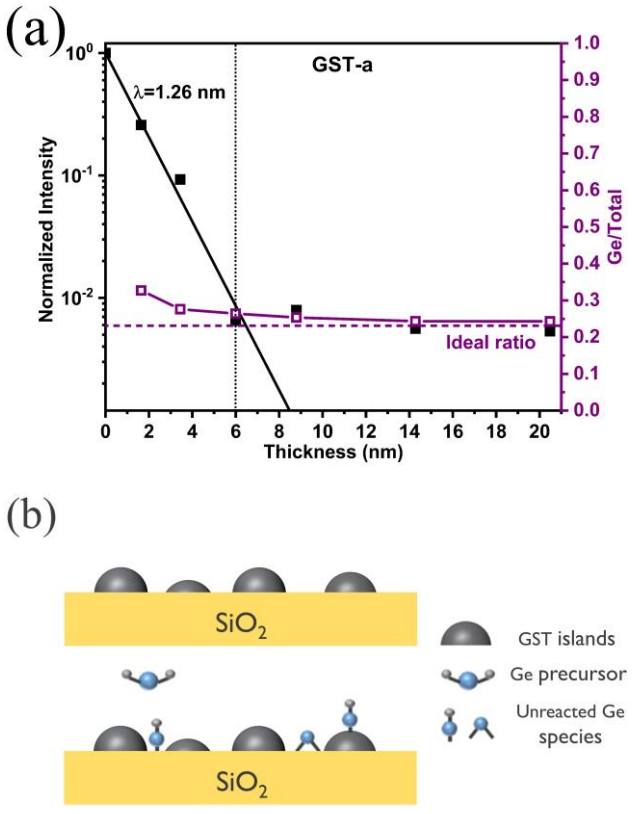

FIG. 9. (a) Comparison of saturation of normalized Si intensity (left axis) with composition ratio (right axis) for GST-a with a purple dotted line indicating the ideal ratio for GST and a black dotted line indicating where the surface gets closed. (b) Schematic showing island growth providing the available active sites on the substrate for incoming precursors of Ge and Sb, resulting in Ge-rich GST.

IV. CONCLUSIONS

This paper discusses the impact of the reaction sequence in ALD of GST on growth per cycle, morphology, and composition. There is no significant effect on density and morphology for GST, while a minor difference in growth per cycle is noted. In terms of composition, a Ge-rich interfacial layer is present at the interface between the SiO_2 substrate and the GST layer, even when starting the deposition with the binary Sb_2Te_3 ALD sequence. This implies that reactions of ALD precursors with the initial SiO_2 substrate affect the initial composition of GST.

T-XRF experiments reveal that $GeCl_2.C_4H_8O_2$ exhibits higher reactivity towards SiO_2 than $SbCl_3$. Moreover, the $Te[(CH_3)_3Si]_2$ precursor reaction with Ge adspecies on the SiO_2 surface yields a Ge-rich surface layer with the Ge/Te ratio of ~4. We propose that the $Te[(CH_3)_3Si]_2$ reaction is limited by either the availability of Cl on the surface or lower reactivity, implying the formation of either -O-Ge-Cl or -O-Ge-O species during $GeCl_2.C_4H_8O_2$ adsorption. Thus, these “unreacted Ge surface species” play a crucial role in forming a Ge-rich interfacial layer during GST ALD starting, regardless of the binary ALD sequence used to start the deposition (GeTe versus Sb_2Te_3). Such species can be formed even when the GST ALD starts with an $SbCl_3$ reaction, as the low reactivity of $SbCl_3$ leads to an incomplete surface coverage. Moreover, the precursors may reach surface sites on the exposed SiO_2 area during several ALD cycles due to island growth leading to a Ge-rich interfacial layer. When the SiO_2 substrate is fully covered, GST reaches the desired composition.

The proposed insights may contribute to optimizing the initial stages of GST ALD on various initial substrates, enabling better composition control and possibly enhancing device

performance. We note that the proposed reaction mechanisms are based on assumptions, as explained above. It would be interesting to verify the proposed mechanism through additional research, such as density functional theory calculations and/or in-situ characterization of the individual precursor reactions. While the formation of unreacted Ge surface species and island growth are supported by quantitative measurement results, the overall Ge profiles are explained only qualitatively in this work. Explaining the quantitative Ge-profiles during ALD for the processes with different starting sequences could require additional investigations, for example by Monte Carlo simulations of the film composition after multiple GST ALD reaction cycles and resulting depth profiles. Moreover, we witnessed a similar Ge-rich interface on TiN substrates, a relevant or heater material for GST in applications.[19] Future studies could therefore consider different precursors, substrates, temperatures, and a greater number of ALD cycles to get a more insight in the reaction mechanisms. This encourages a detailed investigation of the understanding of the substrate effect on GST composition. Nonetheless, this paper underscores the significance of the initial surface reactions in ternary ALD processes and their effect on the growth per cycle and composition. It also opens avenues for further research into reaction sequence in ternary ALD.

ACKNOWLEDGMENTS

We thank Jerome Innocent, Andrea Illiberi, and Michael Givens from ASM Belgium for the GST process. We also thank Alexis Franquet for TOF-SIMS and Praveen Dara for T-XRF characterization and its interpretation.

DATA AVAILABILITY

The data that support the findings of this study are available within the article and its supplementary material.

REFERENCES

[1] S.W. Fong, C.M. Neumann, and H.-S.P. Wong, "Phase-Change Memory—Towards a Storage-Class Memory," IEEE Trans Electron Devices **64**(11), 4374–4385 (2017).
[2] V. Adinolfi, L. Cheng, M. Laudato, R.C. Clarke, V.K. Narasimhan, S. Balatti, S. Hoang, and K.A. Littau, "Composition-Controlled Atomic Layer Deposition of Phase-Change Memories and Ovonic Threshold Switches with High Performance," ACS Nano **13**(9), 10440–10447 (2019).
[3] T. Kim, and S. Lee, "Evolution of Phase-Change Memory for the Storage-Class Memory and Beyond," IEEE Trans Electron Devices **67**(4), 1394–1406 (2020).
[4] I. Boybat, M. Le Gallo, S.R. Nandakumar, T. Moraitis, T. Parnell, T. Tuma, B. Rajendran, Y. Leblebici, A. Sebastian, and E. Eleftheriou, "Neuromorphic computing with multi-memristive synapses," Nature Communications 2018 9:1 **9**(1), 1–12 (2018).
[5] Q. Wang, G. Niu, W. Ren, R. Wang, X. Chen, X. Li, Z.-G. Ye, Y.-H. Xie, S. Song, Z. Song, Q. Wang, G. Niu, W. Ren, R.B. Wang, X.G. Chen, X. Li, S.N. Song, Z.T. Song, Z. Ye, and Y. Xie, "Phase Change Random Access Memory for Neuro-Inspired Computing," Adv Electron Mater **7**(6), 2001241 (2021).
[6] C. Rios, M. Stegmaier, P. Hosseini, D. Wang, T. Scherer, C.D. Wright, H. Bhaskaran, and W.H.P. Pernice, "Integrated all-photonic non-volatile multi-level memory," Nature Photonics 2015 9:11 **9**(11), 725–732 (2015).
[7] H. Zhang, L. Zhou, B.M.A. Rahman, X. Wu, L. Lu, Y. Xu, J. Xu, J. Song, Z. Hu, L. Xu, and J. Chen, "Ultracompact Si-GST hybrid waveguides for nonvolatile light wave manipulation," IEEE Photonics J **10**(1), (2018).
[8] P. Hosseini, C.D. Wright, and H. Bhaskaran, "An optoelectronic framework enabled by low-dimensional phase-change films," Nature 2014 511:7508 **511**(7508), 206–211 (2014).
[9] Y. Cui, Y. Zhang, and Z. Cheng, "Nonvolatile Displays Based on Phase Change Materials," Adv Opt Mater **11**(21), 2300481 (2023).
[10] N. Bala, B. Khan, K. Singh, P. Singh, A.P. Singh, and A. Thakur, "Recent advances in doped Ge2Sb2Te5 thin film based phase change memories," Mater Adv **4**(3), 747–768 (2023).
[11] V. Pore, T. Hatanpää, M. Ritala, and M. Leskelä, "Atomic Layer Deposition of Metal Tellurides and Selenides Using Alkylsilyl Compounds of Tellurium and Selenium," J Am Chem Soc **131**(10), 3478–3480 (2009).
[12] M. Ritala, V. Pore, T. Hatanpää, M. Heikkilä, M. Leskelä, K. Mizohata, A. Schrott, S. Raoux, and S.M. Rossnagel, "Atomic layer deposition of Ge2Sb2Te5 thin films," Microelectron Eng **86**(7–9), 1946–1949 (2009).
[13] S. Song, D. Yao, Z. Song, L. Gao, Z. Zhang, L. Li, L. Shen, L. Wu, B. Liu, Y. Cheng, and S. Feng, "Phase-change properties of GeSbTe thin films deposited by plasma-enchanced atomic layer depositon," Nanoscale Res Lett **10**(1), 1–5 (2015).
[14] T. Eom, T. Gwon, S. Yoo, B.J. Choi, M.-S. Kim, I. Buchanan, S. Ivanov, M. Xiao, and C.S. Hwang, "Combined Ligand Exchange and Substitution Reactions in Atomic Layer Deposition of Conformal $Ge_2Sb_2Te_5$ Film for Phase Change Memory Application," Chemistry of Materials **27**(10), 3707–3713 (2015).
[15] T. Gwon, T. Eom, S. Yoo, C. Yoo, E. Park, S. Kim, M.-S. Kim, I. Buchanan, M. Xiao, S. Ivanov, and C.S. Hwang, "Atomic Layer Deposition of GeTe and Ge–Sb–Te Films Using $HGeCl_3$, $Sb(OC_2H_5)_3$, and $\{(CH_3)_3Si\}_2Te$ and Their Reaction Mechanisms," Chemistry of Materials **29**(19), 8065–8072 (2017).
[16] M. Šilinskas, B. Kalkofen, R. Balasubramanian, A. Batmanov, E.P. Burte, N. Harmgarth, F. Zörner, F.T. Edelmann, B. Garke, and M. Lisker, "Plasma-assisted atomic layer deposition of

germanium antimony tellurium compounds," Journal of Vacuum Science & Technology A: Vacuum, Surfaces, and Films **36**(2), 21510 (2018).
[17] E.-S. Park, C. Yoo, W. Kim, M. Ha, J.W. Jeon, T. Eom, Y.K. Lee, and C.S. Hwang, "Atomic Layer Deposition of Nanocrystalline-As-Deposited $(GeTe)_x (Sb_2Te_3)_{1-x}$ Films for Endurable Phase Change Memory," Chemistry of Materials **31**(21), 8752–8763 (2019).
[18] T. Eom, S. Choi, B.J. Choi, M.H. Lee, T. Gwon, S.H. Rha, W. Lee, M.S. Kim, M. Xiao, I. Buchanan, D.Y. Cho, and C.S. Hwang, "Conformal formation of (GeTe 2) (1- x)(Sb 2Te 3) x layers by atomic layer deposition for nanoscale phase change memories," Chemistry of Materials **24**(11), 2099–2110 (2012).
[19] J. Sinha, L. Gallis, J.-W.J. Clerix, M. van der Veen, J. Innocent, A. Illiberi, M. Givens, L. Nyns, and A. Delabie, "Low-Temperature Dechlorosilylation Chemistry for Area-Selective Deposition of $Ge_2Sb_2Te_5$ and Its Mechanism in Nanopatterns," Chemistry of Materials **36**(12), 5943–5952 (2024).
[20] A. Haider, S. Deng, W. Devulder, J.W. Maes, J.M. Girard, G. Khalil El Hajjam, G.S. Kar, K. Opsomer, C. Detavernier, M. Givens, L. Goux, S. Van Elshocht, R. Delhougne, A. Delabie, M. Caymax, and J. Swerts, "Pulsed chemical vapor deposition of conformal GeSe for application as an OTS selector," Mater Adv **2**(5), 1635–1643 (2021).
[21] K. Knapas, T. Hatanpää, M. Ritala, and M. Leskelä, "In Situ Reaction Mechanism Studies on Atomic Layer Deposition of Sb_2Te_3 and GeTe from $(Et_3Si)_2Te$ and Chlorides," Chemistry of Materials **22**(4), 1386–1391 (2010).
[22] R.L. Puurunen, "Formation of Metal Oxide Particles in Atomic Layer Deposition During the Chemisorption of Metal Chlorides: A Review," Chemical Vapor Deposition **11**(2), 79–90 (2005).
[23] L. Nyns, A. Delabie, M. Caymax, M.M. Heyns, S. Van Elshocht, C. Vinckier, and S. De Gendt, "HfO[sub 2] Atomic Layer Deposition Using HfCl[sub 4]/H[sub 2]O: The First Reaction Cycle," J Electrochem Soc **155**(12), G269 (2008).
[24] J. Soethoudt, F. Grillo, E.A. Marques, J.R. van Ommen, Y. Tomczak, L. Nyns, S. Van Elshocht, and A. Delabie, "Diffusion-Mediated Growth and Size-Dependent Nanoparticle Reactivity during Ruthenium Atomic Layer Deposition on Dielectric Substrates," Adv Mater Interfaces **5**(24), 1800870 (2018).
[25] R.L. Puurunen, "Growth Per Cycle in Atomic Layer Deposition: A Theoretical Model," Chemical Vapor Deposition **9**(5), 249–257 (2003).
[26] M. Al Hareri, and D.J.H. Emslie, "Room-Temperature Atomic Layer Deposition of Elemental Antimony," Chemistry of Materials **34**(5), 2400–2409 (2022).
[27] M.L. Green, M.-Y. Ho, ; B Busch, ; G D Wilk, ; T Sorsch, ; T Conard, ; B Brijs, ; W Vandervorst, ; P I Räisänen, ; D Muller, ; M Bude, ; J Grazul, B. Busch, G.D. Wilk, T. Sorsch, T. Conard, B. Brijs, W. Vandervorst, P.I. Rä Isä Nen, D. Muller, M. Bude, and J. Grazul, "Nucleation and growth of atomic layer deposited HfO2 gate dielectric layers on chemical oxide (Si–O–H) and thermal oxide (SiO2 or Si–O–N) underlayers," J Appl Phys **92**(12), 7168–7174 (2002).
[28] T. Conard, W. Vandervorst, J. Petry, C. Zhao, W. Besling, H. Nohira, and O. Richard, "TOF-SIMS as a rapid diagnostic tool to monitor the growth mode of thin (high k) films," Appl Surf Sci **203–204**, 400–403 (2003).
[29] A. Delabie, R.L. Puurunen, B. Brijs, M. Caymax, T. Conard, B. Onsia, O. Richard, W. Vandervorst, C. Zhao, M.M. Heyns, M. Meuris, M.M. Viitanen, H.H. Brongersma, M. De Ridder, L. V. Goncharova, E. Garfunkel, T. Gustafsson, and W. Tsai, "Atomic layer deposition of hafnium oxide on germanium substrates," J Appl Phys **97**(6), 64104 (2005).